Z. Phys. C 74, 577–586 (1997)

ZEITSCHRIFT
FÜR PHYSIK C

Experimental Physics

Search for new phenomena using single photon events at LEP1

DELPHI Collaboration

P.Abreu[21], W.Adam[50], T.Adye[37], E.Agasi[31], I.Ajinenko[42], R.Aleksan[39], G.D.Alekseev[16], R.Alemany[49], P.P.Allport[22], S.Almehed[24], U.Amaldi[9], S.Amato[47], A.Andreazza[28], M.L.Andrieux[14], P.Antilogus[9], W-D.Apel[17], Y.Arnoud[39], B.Åsman[44], J-E.Augustin[19], A.Augustinus[9], P.Baillon[9], P.Bambade[19], F.Barao[21], R.Barate[14], M.Barbi[47], G.Barbiellini[46], D.Y.Bardin[16], A.Baroncelli[40], O.Barring[24], J.A.Barrio[26], W.Bartl[50], M.J.Bates[37], M.Battaglia[15], M.Baubillier[23], J.Baudot[39], K-H.Becks[52], M.Begalli[6], P.Beilliere[8], Yu.Belokopytov[9,53], K.Beloous[42], A.C.Benvenuti[5], M.Berggren[47], D.Bertrand[2], F.Bianchi[45], M.Bigi[45], M.S.Bilenky[16], P.Billoir[23], D.Bloch[10], M.Blume[52], S.Blyth[35], T.Bolognese[39], M.Bonesini[28], W.Bonivento[28], P.S.L.Booth[22], G.Borisov[42], C.Bosio[40], S.Bosworth[35], O.Botner[48], E.Boudinov[31], B.Bouquet[19], C.Bourdarios[9], T.J.V.Bowcock[22], M.Bozzo[13], P.Branchini[40], K.D.Brand[36], T.Brenke[52], R.A.Brenner[15], C.Bricman[2], L.Brillault[23], R.C.A.Brown[9], P.Bruckman[18], J-M.Brunet[8], L.Bugge[33], T.Buran[33], T.Burgsmueller[52], P.Buschmann[52], A.Buys[9], S.Cabrera[49], M.Caccia[28], M.Calvi[28], A.J.Camacho Rozas[41], T.Camporesi[9], V.Canale[38], M.Canepa[13], K.Cankocak[44], F.Cao[2], F.Carena[9], L.Carroll[22], C.Caso[13], M.V.Castillo Gimenez[49], A.Cattai[9], F.R.Cavallo[5], L.Cerrito[38], V.Chabaud[9], Ph.Charpentier[9], L.Chaussard[25], J.Chauveau[23], P.Checchia[36], G.A.Chelkov[16], M.Chen[2], R.Chierici[45], P.Chliapnikov[42], P.Chochula[7], V.Chorowicz[9], V.Cindro[43], P.Collins[9], J.L.Contreras[19], R.Contri[13], E.Cortina[49], G.Cosme[19], F.Cossutti[46], H.B.Crawley[1], D.Crennell[37], G.Crosetti[13], J.Cuevas Maestro[34], S.Czellar[15], E.Dahl-Jensen[29], J.Dahm[52], B.Dalmagne[19], M.Dam[29], G.Damgaard[29], P.D.Dauncey[37], M.Davenport[9], W.Da Silva[23], C.Defoix[8], A.Deghorain[2], G.Della Ricca[46], P.Delpierre[27], N.Demaria[35], A.De Angelis[9], W.De Boer[17], S.De Brabandere[2], C.De Clercq[2], C.De La Vaissiere[23], B.De Lotto[46], A.De Min[36], L.De Paula[47], C.De Saint-Jean[39], H.Dijkstra[9], L.Di Ciaccio[38], F.Djama[10], J.Dolbeau[8], M.Donszelmann[9], K.Doroba[51], M.Dracos[10], J.Drees[52], K.-A.Drees[52], M.Dris[32], Y.Dufour[9], D.Edsall[1], R.Ehret[17], G.Eigen[4], T.Ekelof[48], G.Ekspong[44], M.Elsing[52], J-P.Engel[10], N.Ershaidat[23], B.Erzen[43], M.Espirito Santo[21], E.Falk[24], D.Fassouliotis[32], M.Feindt[9], A.Fenyuk[42], A.Ferrer[49], T.A.Filippas[32], A.Firestone[1], P.-A.Fischer[10], H.Foeth[9], E.Fokitis[32], F.Fontanelli[13], F.Formenti[9], B.Franek[37], P.Frenkiel[8], D.C.Fries[17], A.G.Frodesen[4], R.Fruhwirth[50], F.Fulda-Quenzer[19], J.Fuster[49], A.Galloni[22], D.Gamba[45], M.Gandelman[6], C.Garcia[49], J.Garcia[41], C.Gaspar[9], U.Gasparini[36], Ph.Gavillet[9], E.N.Gazis[32], D.Gele[10], J-P.Gerber[10], L.Gerdyukov[42], M.Gibbs[22], R.Gokieli[51], B.Golob[43], G.Gopal[37], L.Gorn[1], M.Gorski[51], Yu.Gouz[45,53], V.Gracco[13], E.Graziani[40], G.Grosdidier[19], K.Grzelak[51], S.Gumenyuk[28,53], P.Gunnarsson[44], M.Gunther[48], J.Guy[37], F.Hahn[9], S.Hahn[52], Z.Hajduk[18], A.Hallgren[48], K.Hamacher[52], W.Hao[31], F.J.Harris[35], V.Hedberg[24], J.J.Hernandez[49], P.Herquet[2], H.Herr[9], T.L.Hessing[35], E.Higon[49], H.J.Hilke[9], T.S.Hill[1], S-O.Holmgren[44], P.J.Holt[35], D.Holthuizen[31], S.Hoorelbeke[2], M.Houlden[22], K.Huet[2], K.Hultqvist[44], J.N.Jackson[22], R.Jacobsson[44], P.Jalocha[18], R.Janik[7], Ch.Jarlskog[24], G.Jarlskog[24], P.Jarry[39], B.Jean-Marie[19], E.K.Johansson[44], L.Jonsson[24], P.Jonsson[24], C.Joram[9], P.Juillot[10], M.Kaiser[17], F.Kapusta[23], K.Karafasoulis[11], M.Karlsson[44], E.Karvelas[11], S.Katsanevas[3], E.C.Katsoufis[32], R.Keranen[4], Yu.Khokhlov[42], B.A.Khomenko[16], N.N.Khovanski[16], B.King[22], N.J.Kjaer[29], H.Klein[9], A.Klovning[4], P.Kluit[31], B.Koene[31], P.Kokkinias[11], M.Koratzinos[9], K.Korcyl[18], C.Kourkoumelis[3], O.Kouznetsov[13,16], P.-H.Kramer[52], M.Krammer[50], C.Kreuter[17], I.Kronkvist[24], Z.Krumstein[16], W.Krupinski[18], P.Kubinec[7], W.Kucewicz[18], K.Kurvinen[15], C.Lacasta[49], I.Laktineh[25], S.Lamblot[23], J.W.Lamsa[1], L.Lanceri[46], D.W.Lane[1], P.Langefeld[52], I.Last[22], J-P.Laugier[39], R.Lauhakangas[15], G.Leder[50], F.Ledroit[14], V.Lefebure[2], C.K.Legan[1], R.Leitner[30], Y.Lemoigne[39], J.Lemonne[2], G.Lenzen[52], V.Lepeltier[19], T.Lesiak[36], D.Liko[50], R.Lindner[52], A.Lipniacka[36], I.Lippi[36], B.Loerstad[24], M.Lokajicek[12], J.G.Loken[35], J.M.Lopez[41], D.Loukas[11], P.Lutz[39], L.Lyons[35], J.MacNaughton[50], G.Maehlum[17], A.Maio[21], V.Malychev[16], F.Mandl[50], J.Marco[41], R.Marco[41], B.Marechal[47], M.Margoni[36], J-C.Marin[9], C.Mariotti[40], A.Markou[11], T.Maron[52], C.Martinez-Rivero[41], F.Martinez-Vidal[49], S.Marti i Garcia[49], F.Matorras[41], C.Matteuzzi[9], G.Matthiae[38], M.Mazzucato[36], M.Mc Cubbin[9], R.Mc Kay[1], R.Mc Nulty[22], J.Medbo[48], M.Merk[31], C.Meroni[28], S.Meyer[17], W.T.Meyer[1], M.Michelotto[36], E.Migliore[45], L.Mirabito[25], W.A.Mitaroff[50], U.Mjoernmark[24], T.Moa[44], R.Moeller[29], K.Moenig[9], M.R.Monge[13], P.Morettini[13], H.Mueller[17], L.M.Mundim[6], W.J.Murray[37], B.Muryn[18], G.Myatt[35], F.Naraghi[14], F.L.Navarria[5], S.Navas[49], K.Nawrocki[51], P.Negri[28], S.Nemecek[12], W.Neumann[52], N.Neumeister[50], R.Nicolaidou[3], B.S.Nielsen[29], M.Nieuwenhuizen[31], V.Nikolaenko[10], P.Niss[44], A.Nomerotski[36], A.Normand[35], W.Oberschulte-Beckmann[17], V.Obraztsov[42], A.G.Olshevski[16], A.Onofre[21], R.Orava[15], K.Osterberg[15], A.Ouraou[39], P.Paganini[19], M.Paganoni[9], P.Pages[10], H.Palka[18], Th.D.Papadopoulou[32], K.Papageorgiou[11], L.Pape[9], C.Parkes[35], F.Parodi[13], A.Passeri[40], M.Pegoraro[36], L.Peralta[21], H.Pernegger[50], M.Pernicka[50], A.Perrotta[5], C.Petridou[46], A.Petrolini[13], M.Petrovyck[28,53], H.T.Phillips[37], G.Piana[13], F.Pierre[39], M.Pimenta[21], M.Pindo[28], S.Plaszczynski[19], O.Podobrin[17], M.E.Pol[6], G.Polok[18], P.Poropat[46], V.Pozdniakov[16], M.Prest[46], P.Privitera[38], N.Pukhaeva[16], A.Pullia[28], D.Radojicic[35], S.Ragazzi[28], H.Rahmani[32], J.Rames[12], P.N.Ratoff[20], A.L.Read[33], M.Reale[52], P.Rebecchi[19],

N.G.Redaelli[28], M.Regler[50], D.Reid[9], P.B.Renton[35], L.K.Resvanis[3], F.Richard[19], J.Richardson[22], J.Ridky[12], G.Rinaudo[45], I.Ripp[39], A.Romero[45], I.Roncagliolo[13], P.Ronchese[36], L.Roos[14], E.I.Rosenberg[1], E.Rosso[9], P.Roudeau[19], T.Rovelli[5], W.Ruckstuhl[31], V.Ruhlmann-Kleider[39], A.Ruiz[41], K.Rybicki[18], H.Saarikko[15], Y.Sacquin[39], A.Sadovsky[16], G.Sajot[14], J.Salt[49], J.Sanchez[26], M.Sannino[13], M.Schimmelpfennig[17], H.Schneider[17], U.Schwickerath[17], M.A.E.Schyns[52], G.Sciolla[45], F.Scuri[46], P.Seager[20], Y.Sedykh[16], A.M.Segar[35], A.Seitz[17], R.Sekulin[37], R.C.Shellard[6], I.Siccama[31], P.Siegrist[39], S.Simonetti[39], F.Simonetto[36], A.N.Sisakian[16], B.Sitar[7], T.B.Skaali[33], G.Smadja[25], N.Smirnov[42], O.Smirnova[16], G.R.Smith[37], O.Solovianov[42], R.Sosnowski[51], D.Souza-Santos[6], T.Spassov[21], E.Spiriti[40], P.Sponholz[52], S.Squarcia[13], C.Stanescu[40], S.Stapnes[33], I.Stavitski[36], F.Stichelbaut[9], A.Stocchi[19], J.Strauss[50], R.Strub[10], B.Stugu[4], M.Szczekowski[51], M.Szeptycka[51], T.Tabarelli[28], J.P.Tavernet[23], O.Tchikilev[42], A.Tilquin[27], J.Timmermans[31], L.G.Tkatchev[16], T.Todorov[10], D.Z.Toet[31], A.Tomaradze[2], B.Tome[21], A.Tonazzo[28], L.Tortora[40], G.Transtromer[24], D.Treille[9], W.Trischuk[9], G.Tristram[8], A.Trombini[19], C.Troncon[28], A.Tsirou[9], M-L.Turluer[39], I.A.Tyapkin[16], M.Tyndel[37], S.Tzamarias[22], B.Ueberschaer[52], O.Ullaland[9], V.Uvarov[42], G.Valenti[5], E.Vallazza[9], C.Vander Velde[2], G.W.Van Apeldoorn[31], P.Van Dam[31], W.K.Van Doninck[2], J.Van Eldik[31], N.Vassilopoulos[35], G.Vegni[28], L.Ventura[36], W.Venus[37], F.Verbeure[2], M.Verlato[36], L.S.Vertogradov[16], D.Vilanova[39], P.Vincent[25], L.Vitale[46], E.Vlasov[42], A.S.Vodopyanov[16], V.Vrba[12], H.Wahlen[52], C.Walck[44], M.Weierstall[52], P.Weilhammer[9], C.Weiser[17], A.M.Wetherell[9], D.Wicke[52], J.H.Wickens[2], M.Wielers[17], G.R.Wilkinson[35], W.S.C.Williams[35], M.Winter[10], M.Witek[18], K.Woschnagg[48], K.Yip[35], O.Yushchenko[42], F.Zach[25], A.Zaitsev[42], A.Zalewska[18], P.Zalewski[51], D.Zavrtanik[43], E.Zevgolatakos[11], N.I.Zimin[16], M.Zito[39], D.Zontar[43], R.Zuberi[35], G.C.Zucchelli[44], G.Zumerle[36]

[1] Ames Laboratory and Department of Physics, Iowa State University, Ames IA 50011, USA
[2] Physics Department, Univ. Instelling Antwerpen, Universiteitsplein 1, B-2610 Wilrijk, Belgium and IIHE, ULB-VUB, Pleinlaan 2, B-1050 Brussels, Belgium and Faculté des Sciences, Univ. de l'Etat Mons, Av. Maistriau 19, B-7000 Mons, Belgium
[3] Physics Laboratory, University of Athens, Solonos Str. 104, GR-10680 Athens, Greece
[4] Department of Physics, University of Bergen, Allégaten 55, N-5007 Bergen, Norway
[5] Dipartimento di Fisica, Università di Bologna and INFN, Via Irnerio 46, I-40126 Bologna, Italy
[6] Centro Brasileiro de Pesquisas Físicas, rua Xavier Sigaud 150, RJ-22290 Rio de Janeiro, Brazil and Depto. de Física, Pont. Univ. Católica, C.P. 38071 RJ-22453 Rio de Janeiro, Brazil and Inst. de Física, Univ. Estadual do Rio de Janeiro, rua São Francisco Xavier 524, Rio de Janeiro, Brazil
[7] Comenius University, Faculty of Mathematics and Physics, Mlynska Dolina, SK-84215 Bratislava, Slovakia
[8] Collège de France, Lab. de Physique Corpusculaire, IN2P3-CNRS, F-75231 Paris Cedex 05, France
[9] CERN, CH-1211 Geneva 23, Switzerland
[10] Centre de Recherche Nucléaire, IN2P3 - CNRS/ULP - BP20, F-67037 Strasbourg Cedex, France
[11] Institute of Nuclear Physics, N.C.S.R. Demokritos, P.O. Box 60228, GR-15310 Athens, Greece
[12] FZU, Inst. of Physics of the C.A.S. High Energy Physics Division, Na Slovance 2, 180 40, Praha 8, Czech Republic
[13] Dipartimento di Fisica, Università di Genova and INFN, Via Dodecaneso 33, I-16146 Genova, Italy
[14] Institut des Sciences Nucléaires, IN2P3-CNRS, Université de Grenoble 1, F-38026 Grenoble Cedex, France
[15] Research Institute for High Energy Physics, SEFT, P.O. Box 9, FIN-00014 Helsinki, Finland
[16] Joint Institute for Nuclear Research, Dubna, Head Post Office, P.O. Box 79, 101 000 Moscow, Russian Federation
[17] Institut für Experimentelle Kernphysik, Universität Karlsruhe, Postfach 6980, D-76128 Karlsruhe, Germany
[18] Institute of Nuclear Physics and University of Mining and Metalurgy, Ul. Kawiory 26a, PL-30055 Krakow, Poland
[19] Université de Paris-Sud, Lab. de l'Accélérateur Linéaire, IN2P3-CNRS, Bât. 200, F-91405 Orsay Cedex, France
[20] School of Physics and Materials, University of Lancaster, Lancaster LA1 4YB, UK
[21] LIP, IST, FCUL - Av. Elias Garcia, 14-1^{o}, P-1000 Lisboa Codex, Portugal
[22] Department of Physics, University of Liverpool, P.O. Box 147, Liverpool L69 3BX, UK
[23] LPNHE, IN2P3-CNRS, Universités Paris VI et VII, Tour 33 (RdC), 4 place Jussieu, F-75252 Paris Cedex 05, France
[24] Department of Physics, University of Lund, Sölvegatan 14, S-22363 Lund, Sweden
[25] Université Claude Bernard de Lyon, IPNL, IN2P3-CNRS, F-69622 Villeurbanne Cedex, France
[26] Universidad Complutense, Avda. Complutense s/n, E-28040 Madrid, Spain
[27] Univ. d'Aix - Marseille II - CPP, IN2P3-CNRS, F-13288 Marseille Cedex 09, France
[28] Dipartimento di Fisica, Università di Milano and INFN, Via Celoria 16, I-20133 Milan, Italy
[29] Niels Bohr Institute, Blegdamsvej 17, DK-2100 Copenhagen 0, Denmark
[30] NC, Nuclear Centre of MFF, Charles University, Areal MFF, V Holesovickach 2, 180 00, Praha 8, Czech Republic
[31] NIKHEF-H, Postbus 41882, NL-1009 DB Amsterdam, The Netherlands
[32] National Technical University, Physics Department, Zografou Campus, GR-15773 Athens, Greece
[33] Physics Department, University of Oslo, Blindern, N-1000 Oslo 3, Norway
[34] Dpto. Fisica, Univ. Oviedo, C/P. Pérez Casas, S/N-33006 Oviedo, Spain
[35] Department of Physics, University of Oxford, Keble Road, Oxford OX1 3RH, UK
[36] Dipartimento di Fisica, Università di Padova and INFN, Via Marzolo 8, I-35131 Padua, Italy
[37] Rutherford Appleton Laboratory, Chilton, Didcot OX11 OQX, UK
[38] Dipartimento di Fisica, Università di Roma II and INFN, Tor Vergata, I-00173 Rome, Italy
[39] Centre d'Etudes de Saclay, DSM/DAPNIA, F-91191 Gif-sur-Yvette Cedex, France
[40] Istituto Superiore di Sanità, Ist. Naz. di Fisica Nucl. (INFN), Viale Regina Elena 299, I-00161 Rome, Italy
[41] Instituto de Fisica de Cantabria (CSIC-UC), Avda. los Castros, S/N-39006 Santander, Spain, (CICYT-AEN93-0832)
[42] Inst. for High Energy Physics, Serpukov P.O. Box 35, Protvino, (Moscow Region), Russian Federation
[43] J. Stefan Institute and Department of Physics, University of Ljubljana, Jamova 39, SI-61000 Ljubljana, Slovenia
[44] Fysikum, Stockholm University, Box 6730, S-113 85 Stockholm, Sweden
[45] Dipartimento di Fisica Sperimentale, Università di Torino and INFN, Via P. Giuria 1, I-10125 Turin, Italy
[46] Dipartimento di Fisica, Università di Trieste and INFN, Via A. Valerio 2, I-34127 Trieste, Italy and Istituto di Fisica, Università di Udine, I-33100 Udine, Italy
[47] Univ. Federal do Rio de Janeiro, C.P. 68528 Cidade Univ., Ilha do Fundão BR-21945-970 Rio de Janeiro, Brazil

[48] Department of Radiation Sciences, University of Uppsala, P.O. Box 535, S-751 21 Uppsala, Sweden
[49] IFIC, Valencia-CSIC, and D.F.A.M.N., U. de Valencia, Avda. Dr. Moliner 50, E-46100 Burjassot (Valencia), Spain
[50] Institut für Hochenergiephysik, Österr. Akad. d. Wissensch., Nikolsdorfergasse 18, A-1050 Vienna, Austria
[51] Inst. Nuclear Studies and University of Warsaw, Ul. Hoza 69, PL-00681 Warsaw, Poland
[52] Fachbereich Physik, University of Wuppertal, Postfach 100 127, D-42097 Wuppertal 1, Germany
[53] On leave of absence from IHEP Serpukhov

Received: 24 January 1996 / Revised version: 14 January 1997

Abstract. Data are presented on the reaction $e^+e^- \to \gamma$ + no other detected particle at centre-of-mass energies of 89.48, 91.26 and 93.08 GeV. The cross-section for this reaction is related directly to the number of light neutrino generations which couple to the Z^0 boson, and to several other possible phenomena such as the production of excited neutrinos, the production of any invisible 'X' particle, and the magnetic moment of the tau neutrino. Based on the observed number of single photon events, the number of light neutrinos that couple to the Z^0 is measured to be N_ν = 2.89 $\pm$ 0.38. No evidence is found for anomalous production of energetic single photons, and upper limits at 95% confidence level are determined for excited neutrino production (BR $< 4 - 8 \times 10^{-6}$ depending on its mass), production of an invisible 'X' particle ($\sigma < 0.1$ pb for masses below 60 GeV), and the magnetic moment of the tau neutrino ($< 5.1 \times 10^{-6} \mu_B$).

1 Introduction

This paper reports a study of the reaction $e^+e^- \to \gamma$ and no other detected particle, using data taken by the DELPHI detector [1, 2] at the CERN LEP1 collider in 1993-1994.

The rate of such events can be used to estimate the number of light neutrino generations which couple to the Z^0 via the reaction $e^+e^- \to \nu\bar{\nu}\gamma$ [3, 4, 5, 6, 7, 8]. In principle such a study may also provide a clear signal for new phenomena, such as the existence of excited neutrinos [9], a possible magnetic moment for the tau neutrino [10], and on the production of an invisible 'X' particle in association with a photon, or else provide upper limits on these effects.

In Sect. 2, aspects of the DELPHI detector pertinent to this analysis are presented. Section 3 presents the data sample and event selection criteria. The uncertainties and backgrounds are discussed in Sect. 4. In Sect. 5, results on the number of light neutrino generations are presented. Results on searches for new physics, including excited neutrinos, the tau neutrino magnetic moment, and an invisible 'X' particle, are presented in Sect. 6. Lastly, the conclusions are summarised.

2 The DELPHI detector

This search for single photon events depends mainly on the features of the barrel electromagnetic calorimeter, the High-density Projection Chamber (HPC) [11], and of the single-photon trigger it provides. The rest of the DELPHI detector is used to establish the absence of any other particles in the final state and to measure the integrated luminosity.

The HPC is a gas sampling calorimeter which uses a long drift time to provide complete three-dimensional energy-deposition information in the manner of a time-projection chamber. It subtends the angular range $41^\circ < \vartheta < 139^\circ$, where ϑ is the polar angle to the beam direction, and it is mounted directly inside the 5.2-metre (inner diameter) superconducting solenoid of DELPHI, which provides a 1.23 Tesla axial magnetic field. The HPC consists of 144 modules arranged in 24 azimuthal sectors, where each sector consists of six modules along the beam axis. Each module consists of 41 layers of lead radiator, totalling about 18 radiation lengths (X_0) at normal incidence, interspersed with 40 gas sampling slots containing a mixture of argon and methane gases. Charge due to ionization produced in the electromagnetic showers drifts along the beam (z) axis in parallel electric and magnetic fields, and is read out via a grid of 128 cathode pads per module, which provides nine samplings along the shower axis. The 15 MHz sampling frequency corresponds to a cell size of 3.5 mm along the beam axis, giving a spatial resolution in z varying between 1.3 and 3.1 mm according to the polar angle. The granularity in the azimuthal angle (ϕ) is about 20 mrad.

The energy resolution of the HPC has been determined [2] from studies of a) $e^+e^- \to e^+e^-$ Bhabha events, giving 45 GeV electromagnetic showers, and b) $e^+e^- \to e^+e^-\gamma$ virtual Compton scatter events, in which the photon is detected in the forward electromagnetic calorimeters, the scattered electron or positron produces an electromagnetic shower in the HPC, and the unscattered positron or electron remains undetected inside the beampipe. In these virtual Compton scatter events, the energies of the scattered electrons and positrons can be calculated precisely from the angles and lie predominantly between 2 and 20 GeV. The electron energy resolution of the HPC determined in this way is $\sigma/\mathrm{E} = 0.043 \oplus 0.32/\sqrt{\mathrm{E}}$, where the symbol $\oplus$ means addition in quadrature, E is in GeV [2], and the effects of about 0.7 X_0 of material in front of the HPC are included.

The DELPHI single photon trigger uses a positive correlation between a signal from the HPC first-level trigger, which comes from a layer of plastic scintillator inserted in each module near shower maximum, and a signal from the HPC second-level trigger, which uses the pattern of charge observed in the module itself. The scintillator provides a fast (< 2 μsec) first-level trigger from each module. To provide a second-level trigger, signals from the cathode pads, which represent the energy deposited in the gas by the shower, are split. They are sent to the FADC's for digitization, and they also provide input to the second level trigger. For the second level trigger, the signals from the 18432 HPC cathode pads are added in groups of 16 to provide 8 signals per module (1152 for the entire HPC). To keep the background levels low, the correlation between the first and second level trig-

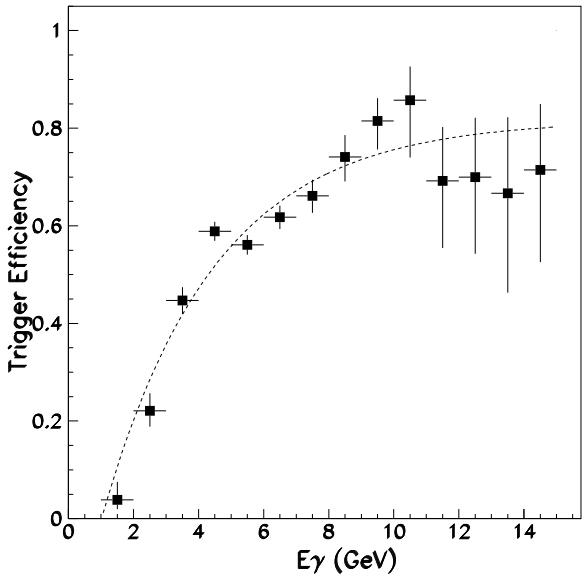

Fig. 1. Efficiency of the HPC single-photon trigger as a function of energy, as determined from scattered electrons and positrons in virtual Compton events. The *dashed curve* shows the result of a fit to the function $\epsilon(E_\gamma) = A - Ce^{-E_\gamma/B}$ with A = 0.82 $\pm$ 0.04, B = 3.46 $\pm$ 0.43 GeV, and C = 1.10 $\pm$ 0.05

gers is performed on groups of three adjacent HPC modules at the same azimuth. For details see reference [12].

The trigger efficiency has been determined in an analysis using the scattered electron or positron in about 8000 virtual Compton events that were triggered independently of the HPC, i.e. with a charged particle trigger. The result is shown in Fig. 1. This measurement is an update of an earlier measurement by the same method which used only the 1993 data [12]. The parametrization of the trigger efficiency shown in Fig. 1, with parameters as given in the figure caption, is used in all subsequent calculations. The systematic uncertainty in the measured cross-sections due to the trigger efficiency, determined from the fit shown in Fig. 1, averages to 4.9% over the observed single photon events. It is included in all cross-section uncertainties quoted below. These efficiencies are measured for an electron or positron incident in the HPC, rather than a photon, but Monte Carlo shower simulations indicate that the corresponding differences in longitudinal shower development are detectable only in the first pad layer of the HPC, and are negligible in this analysis. The simulations show [12] that the width of the threshold shown in Fig. 1 is due both to shower fluctuations and to threshold non-uniformity between different HPC modules.

Measurement of cross-sections requires knowledge of the integrated luminosity. The Small Angle Tagger (SAT) [1] was the main luminosity monitor in DELPHI before the 1994 run. It consisted of two cylindrical calorimeters placed $\pm$232.5 cm from the beam interaction point and covering the polar angular region from 43 mrad to 135 mrad. Each cylinder was composed of a set of circular sheets of lead and scintillating fibres arranged inside an aluminum support. The total depth was equivalent to 20 X_0. On one side, a tungsten mask defined the inner radius of the detector with high precision (20 μm) and prevented off-momentum particles from entering the calorimeter through the internal surface. The read-out segmentation was defined by 3 cm rings in the radial (r) coordinate, 7.5° in ϕ for the four outermost rings, and 15° in ϕ for the others. The energy resolution was $\sigma/\mathrm{E} = 0.012 \oplus 0.114/\sqrt{\mathrm{E}} + 0.023$, where E is in GeV [1].

For the 1994 run, a new luminosity monitor, the Small Angle TIle Calorimeter (STIC) [2] was installed in the DELPHI detector, replacing the SAT. It consists of two identical calorimeters with radial and azimuthal segmentation located at $\pm$220 cm from the interaction point, with an angular coverage between 29 and 185 mrad. Each STIC detector is a lead-scintillator sampling calorimeter (49 layers of 3.4 mm steel laminated lead plates and 3 mm thick scintillator plates giving a total of $\sim$ 27 X_0) with wavelength shifter fibre readout, and is equipped with two planes of silicon strip detectors placed after 4 and 7.4 radiation lengths. The geometry of each calorimeter is projective with respect to the interaction point, and in 1994 the lower radial acceptance was again defined by a tungsten mask placed in front of one of the calorimeters. The experimental uncertainty in the measured luminosity was less than 0.1%, below the theoretical uncertainty of 0.16%. Test beam measurements gave an energy resolution of $\sigma/\mathrm{E} = 0.0152 \oplus 0.135/\sqrt{\mathrm{E}}$, with E in GeV. At 45.6 GeV the measured energy resolution is σ/E =2.7% [2].

The DELPHI Forward Electromagnetic Calorimeter (FEMC) [2] subtends a polar angle $10° < \vartheta < 37°$ and $143° < \vartheta < 170°$. It consists of two 5 m diameter disks with a total of 9064 lead glass blocks in the form of truncated pyramids arranged to point just 3° from the interaction point. The lead glass counters (20 X_0 deep, 5×5 cm^2, $\sim 1° \times 1°$) are read out with vacuum photodiodes. The electron energy resolution is $\sigma/\mathrm{E} = 0.03 \oplus 0.12/\sqrt{\mathrm{E}} \oplus 0.11/\mathrm{E}$, with E in GeV, the last term being due to amplification noise. The resolution quoted includes the degradation due to the two radiation lengths of material in front of the calorimeter. Electron showers at 45 GeV from Bhabha scatter events are measured with σ/E = 4.8%.

The principal source of background to the reaction $e^+e^- \to \nu\bar{\nu}\gamma$ is the radiative Bhabha reaction $e^+e^- \to e^+e^-\gamma$ in which the final state electron and positron both escape detection. This could occur in the 1993 data if the electron and positron emerged at angles below the SAT acceptance ($\vartheta < 43$ mrad) or in the uninstrumented region between the SAT and the forward electromagnetic calorimeter (FEMC), i.e. 135 mrad $< \vartheta <$ 173 mrad. In the 1994 data, the replacement of the SAT by the STIC both improved the small angle acceptance and completely closed the gap between the luminosity monitor and the FEMC.

The DELPHI tracking system [1, 2] is divided into a number of independent devices which include the vertex detector (VD), inner detector (ID), time projection chamber (TPC), and outer detector (OD) in the barrel region, plus forward chambers A and B which enhance tracking closer to the beam direction. The polar angle range covered by the charged particle tracking system is $11° < \vartheta < 169°$. Detailed descriptions of these detectors are found in reference [2]

Table 1. Integrated luminosity at the three centre-of-mass energies

$\sqrt{s}$ (GeV)	$\int \mathscr{L}$ dt (pb^{-1})
89.48	7.532 ± 0.006
91.26	52.462 ± 0.032
93.08	7.645 ± 0.008
Total	67.639 ± 0.034

Table 2. Results of the visual scan

Scan Result	Number of Events
Single photon	106
Alpha	12
Cosmic	13
Noise	1
$e^+e^- \to \gamma\gamma(\gamma)$	5
$e^+e^- \to e^+e^-$	2
Total	139

3 Data sample and event selection

This analysis is based on data collected during the second half of 1993 and throughout 1994. The start date is necessitated by the absence of a true single photon trigger in DELPHI before then.

In a scan of the Z^0 peak during the 1993 run, data were recorded at three centre-of-mass energies, $\sqrt{s}$ = 89.48, 91.26 and 93.08 GeV. The 1994 run was entirely at $\sqrt{s}$ = 91.2 GeV. The integrated luminosities during the period in which the DELPHI single photon trigger was operational in 1993 and 1994 were determined by measuring Bhabha scattering at very small angles using the small angle tagger (SAT) for the 1993 run, and the scintillating tile calorimeter (STIC) for the 1994 run. The integrated luminosities for those runs in which both the TPC and HPC were fully operational and which were used in this analysis are shown in Table 1.

This analysis used single photon events where the photon was detected in the HPC electromagnetic calorimeter. The data sample was defined by the following requirements:

(a) the event had to be triggered by the single photon trigger described earlier, and there had to be no reconstructed charged particle track anywhere in the detector;
(b) the most energetic neutral particle (ie calorimeter shower) had to be measured in the HPC, e.g. not in the hadron calorimeter;
(c) the measured energy E_γ of the shower in the HPC had to be above 3 GeV; and
(d) $|\cos\vartheta_\gamma|$ had to be below 0.7, where ϑ_γ is the polar angle of the shower with respect to the e^+e^- beam interaction point.

Selections (c) and (d) defined the kinematic region of interest. For photon energies below 3 GeV or photon polar angles ϑ_γ below 45°, radiative Bhabha background (see section 4) dominated the $\nu\bar{\nu}\gamma$ signal. In addition:

(e) the shower had to contain energy clusters in at least three of the nine pad layers of the HPC module;
(f) the first energy cluster of the shower had to be in one of the first two pad layers of the HPC module;
(g) the shower could contain no more than one empty row before the end of the shower development; and
(h) no single pad layer of the HPC could contain more than 90% of the total shower energy.

Selections (e) through (h) ensured a clean electromagnetic shower in the HPC, and in particular they discriminated against alpha decays from radioactive inclusions in the HPC lead converter. Also:

(i) there should be no significant evidence of any other neutral particle in the event, i.e. a second calorimeter shower would veto the event if either (a) it was in the HPC, had $E > 0.5$ GeV, passed selections (e) and (h) above, and was more than 20° from the candidate photon, or (b) it was in the hadron calorimeter, forward electromagnetic calorimeter, or luminosity monitor (SAT or STIC), had $E > 2$ GeV, and was more than 20° from the candidate photon.

Cut (i) removed most of the two-photon and three-photon events. The 20° algorithm was used, rather than a blanket veto by any second neutral, because the HPC pattern recognition occasionally produces small satellite showers close to an energetic primary neutral shower. Finally:

(j) the azimuthal and polar angles of the shower axis, as determined in a fit to the spatial distribution of the individual charge clusters in the HPC, each had to be within 15° of the azimuthal and polar angles of the line from the e^+e^- beam interaction point to the shower charge barycentre.

A total of 139 events survived the above cuts. They were all scanned by physicists in two independent scans to verify the presence of a single electromagnetic shower in the HPC electromagnetic calorimeter, and the absence of evidence of any other particles in the event. The event assignments in the two scans were identical for all events classified in either scan as a single photon event. The results of the scan are shown in Table 2.

Most of the rejected events were due to cosmic rays or residual alpha decays. Although shower shape criteria (e) through (h) removed most of the alpha decay events, the occasional juxtaposition of several alpha decays in the same HPC module did cause occasional failures in this algorithm. However, the resulting anomalous shower shape (three or more narrow charge depositions in the same HPC module) was easy to identify visually.

The typical pattern of several aligned hits in detectors other than the HPC (e.g. muon chambers and hadron calorimeter) made most of the surviving cosmic ray events also easy to identify visually. However, a certain fraction of the cosmic ray events were sufficiently out of time with the e^+e^- beam crossing that insufficient hits were reconstructed to allow even visual identification. To evaluate this effect, Fig. 2 shows the differences in polar and azimuthal angles between the shower axis and the line to the shower barycentre, separately for events identified in a much larger scan [1] as single photon events and as cosmic ray events. On the basis of the shapes of the distributions shown in Fig. 2 and the number of cosmic ray events listed in Table 2, the irreducible background to the single photon sample from cosmic

[1] The scan was performed on an event sample that included the 139 events referred to above and was selected with similar but looser cuts

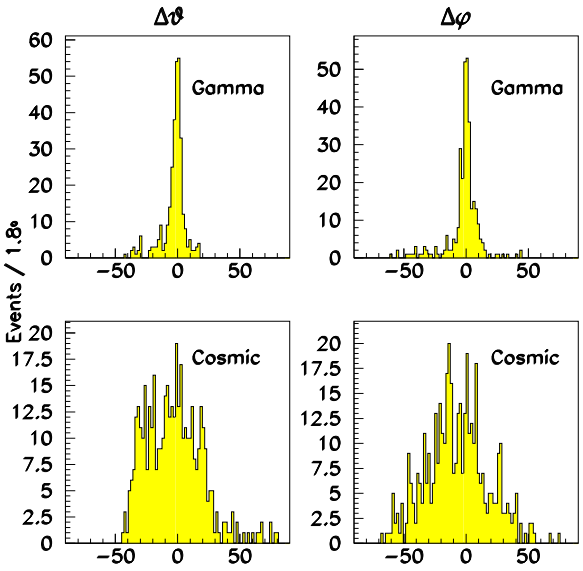

Fig. 2. Distributions in the differences in polar and azimuthal angles (in degrees) between the shower axis and the line to the shower barycentre for single photon events and for events produced by cosmic rays

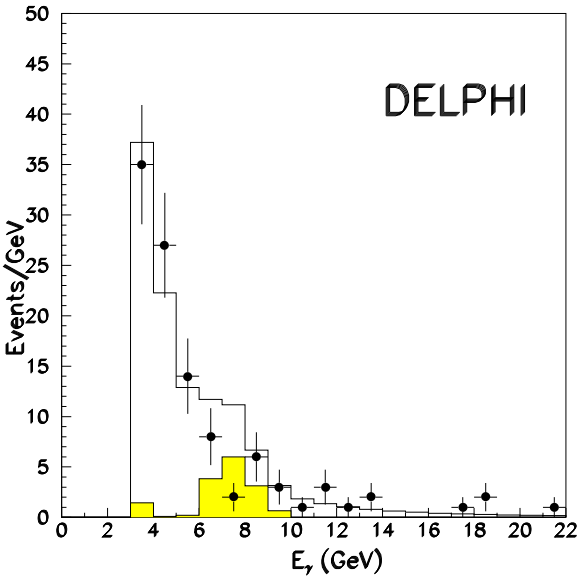

Fig. 3. Distribution in energy of the single photon events (*points*). The *histogram* shows the distribution expected from the signal $\nu\bar{\nu}\gamma$ events plus the background $e^+e^-\gamma$ events (*shaded region*) in which the final state positron and electron both escape detection

Table 3. Upper part: Predicted cross-sections and numbers of events expected for the reaction $e^+e^- \to \nu\bar{\nu}\gamma$ in the kinematic region $E_\gamma > 3$ GeV and $|\cos\vartheta_\gamma| < 0.7$, expected numbers of $e^+e^-\gamma$ background events, and total numbers of single-photon events expected. Lower part: Numbers of events observed, the average efficiencies $<\epsilon>$ including both trigger and reconstruction efficiencies, and the numbers $N^{\nu\bar{\nu}\gamma}_{corrected}$ of $\nu\bar{\nu}\gamma$ events found from the data after subtracting the calculated $e^+e^-\gamma$ background and applying the efficiency corrections

$\sqrt{s}$ =	89.48 GeV	91.26 GeV	93.08 GeV
Predicted σ (pb) (N_ν = 3)	2.3	4.4	11.7
Calculated N_{events}			
$e^+e^- \to \nu\bar{\nu}\gamma$	4.0 ± 0.2	65.5 ± 4.9	23.1 ± 1.8
$e^+e^- \to e^+e^-\gamma$	4.4 ± 0.4	6.5 ± 0.7	3.4 ± 0.3
$N_{expected}$	8.4 ± 0.5	72.0 ± 5.0	26.5 ± 1.8
$N_{observed}$	9	73	24
$<\epsilon>$	0.24	0.28	0.28
$N^{\nu\bar{\nu}\gamma}_{corrected}$	19 ± 13	238 ± 32	74 ± 20
$\sigma(\nu\bar{\nu}\gamma)$ (pb)	2.5 ± 1.7	4.5 ± 0.6	9.7 ± 2.6

ray events in which the cosmic ray particle leaves no clearly identifiable pattern of isolated hits was expected to amount to two events or less.

The final sample of single photon events passing all of the cuts described above was 106 events. Since none was found in the scan to be ambiguous between the single photon hypothesis and any other hypothesis, the systematic uncertainty from the scan was estimated to be less than 3/106 = 2.8% at the 95% confidence level.

Figure 3 shows the distribution in photon energy of the single photon events. The histograms show the predictions for $\nu\bar{\nu}\gamma$ and $e^+e^-\gamma$ events as described below, including all cuts and efficiencies. The double peak structure in the $e^+e^-\gamma$ background distribution corresponds to final state electrons and positrons which escape detection, either by going down the beam pipe or, for the 1993 data only, into the then-uninstrumented region between the SAT and the FEMC.

4 Uncertainties and backgrounds

Apart from the integrated luminosity discussed earlier and the statistical uncertainty in the number of events observed, measurement of a cross-section requires knowledge of the trigger and reconstruction efficiencies.

The trigger efficiency has been discussed in Sect. 2. The efficiency for detecting photons in the accepted region of the HPC, i.e. $E_\gamma > 3$ GeV and $|\cos\vartheta_\gamma| < 0.7$, is less than unity because (i) even within this region there are dead spaces between HPC modules, so that a photon may enter a dead region and fail to be detected, and (ii) the criteria for labelling a signal in the HPC as a legitimate electromagnetic shower are less than 100% efficient, even for photons of energy greater than 3 GeV/c. This arises partly because statistical fluctuations in the energy deposited in a single pad row are occasionally large enough that the entire shower may fail selection criteria (e) through (h), and also because some photons convert in the material of the detector before the HPC. Those that convert before the TPC usually produce reconstructed charged particle tracks, so the event is rejected. But those that convert closer to the HPC, e.g. in the outer detector [2], are often still reconstructed as single neutral showers in the HPC.

The photon detection and reconstruction efficiency was calculated by generating large numbers of single photon events in a series of bins in $\cos\vartheta$, but uniform in azimuthal angle. These events were passed through the standard DELPHI detector simulation and event reconstruction codes. The efficiency was estimated as the fraction of those accepted by the trigger that passed all the single photon selection criteria. Systematic errors arise from uncertainties in edge effects near the boundaries of the HPC modules and the finite energy resolution of the calorimeter. For $E_\gamma > 3$ GeV, the single photon detection and reconstruction efficiency was found to vary from 40% to 70%, its energy dependence be-

ing parametrized by the function

$$\epsilon(E_\gamma) = A - Ce^{-E_\gamma/B} \quad (1)$$

where A = 0.70 $\pm$ 0.02, B = 2.51 $\pm$ 0.65, and C = 0.99 $\pm$ 0.27. This detection and reconstruction efficiency includes all effects described above, except for the single photon trigger efficiency, which has a similar energy dependence and is described in Sect. 2.

There are four possibly significant physics backgrounds: *(i)* a charged particle, e.g. an electron, may arrive at the HPC undetected by all the tracking detectors and produce an electromagnetic shower, which would then be misidentified as due to a photon, but Monte Carlo calculations indicate that this would contribute less than 0.1 events, *(ii)* $e^+e^- \to e^+e^-\gamma$ radiative Bhabha scatters in which the photon satisfies the cuts and the final state electron and positron escape detection, typically by going down the beam pipe or into a crack in the detector, *(iii)* $e^+e^- \to \gamma\gamma$ events in which the second photon escapes detection, and *(iv)* $e^+e^- \to \gamma\gamma\gamma$ events in which two of the photons escape detection.

Estimating the contribution from *(ii)* radiative Bhabha scattering involves detailed Monte Carlo generation of radiative Bhabha scatters including radiative corrections [13], and detailed simulation of the apparatus to include properly all the effects related to whether or not the outgoing electron or positron is detected and thus can veto the event. However, although radiative Bhabha scattering has a total cross-section much greater than that for $\nu\bar{\nu}\gamma$, it results in a photon angular distribution that is much more strongly peaked in the forward-backward direction. The fraction of radiative Bhabha scatters with a photon produced at an angle to the beam direction, $\vartheta_\gamma > \vartheta_{min}$, is

$$f(\vartheta_{min}) \approx \frac{m_e^2}{\vartheta_{min}^2 \cdot \mathrm{E}_{beam}^2} \quad (2)$$

Consequently, the strict energy and angle cuts on the photon ($\mathrm{E}_\gamma > 3$ GeV and $|\cos\vartheta_\gamma| < 0.7$), together with the rejection of events with reconstructed charged particles or high energy deposition in the forward calorimeters, reduce the background from radiative Bhabha scatters to a low level (see next section and Table 3).

The cross-section for *(iii)*, electron-positron annihilation into two photons, is large and is given by:

$$\frac{d\sigma}{dy}(e^+e^- \to \gamma\gamma) = \frac{2\pi\alpha^2}{s} \cdot \frac{1+y^2}{1-y^2} \quad (3)$$

where $y = \cos\vartheta_\gamma$. The two photons are both energetic ($\mathrm{E}_\gamma = \sqrt{s}/2$), and are emitted in opposite directions. Because of the symmetry of the detector, the probability of exactly one of them escaping detection is very low. Since process *(iv)*, $e^+e^- \to \gamma\gamma\gamma$, is mostly the same as the two-photon reaction with the third photon being due to initial state radiation, one of the three photons is generally forward and of relatively low energy, so it may easily escape detection. In addition, the other two photons no longer need to be back-to-back. The symmetry of the detector then increases the probability of losing one of them in a crack and detecting the other. Cut (i) described in section 3 removes most of the two-γ and three-γ events. A few events survive it because a photon occasionally fails to reconstruct as a neutral shower. But then it can be detected in the visual scan as isolated hits in the calorimeters. Monte Carlo calculations [13], including the same cuts and efficiencies as for the data, predict a contribution of 4.2 two-γ and three-γ events, consistent with the five such events identified in the scan (see Table 2). Thus the contamination from $e^+e^- \to \gamma\gamma(\gamma)$ events in the sample labelled single γ events is negligible.

Other possible backgrounds include $e^+e^- \to \mu^+\mu^-\gamma$ and $e^+e^- \to \tau^+\tau^-\gamma$, which have been measured (see [14]), and $e^+e^- \to \gamma\pi^0$, $e^+e^- \to \gamma n\bar{n}$ and $e^+e^- \to \gamma\pi^0\pi^0$, for which there are theoretical expectations [14]. These have all been calculated and found to be negligible in the accepted kinematic region. In addition, a calculation of potential backgrounds from resonances which are produced in two-photon interactions and decay into several π^0's, only one photon from which is detected, shows that this effect is negligible with the severe cuts imposed. Lastly, the higher order reaction $e^+e^- \to \nu\bar{\nu}\gamma\gamma$ has been computed, and found to be negligible.

5 The number of light neutrino generations

In the reaction $e^+e^- \to \nu\bar{\nu}\gamma$, the photon is the result of initial state radiation by either the electron or the positron, and the $\nu\bar{\nu}$ pair is produced either by the decay of a Z^0 boson produced in the s-channel or by W-exchange in the t-channel. In addition, the s-channel and t-channel amplitudes interfere. The suggestion to use this reaction to determine the number of light neutrino generations which couple to the Z^0 has been made many times [3, 4, 5, 6, 7, 8].

The number of light neutrino generations, N_ν, may be calculated from the cross-section for the reaction $e^+e^- \to \nu\bar{\nu}\gamma$ in a specific kinematic region, since the dependence of the doubly differential cross-section on N_ν is known. It is given in reference [5] as

$$\frac{d^2\sigma}{dxdy} = \frac{G_F^2\alpha s(1-x)[(1-x/2)^2 + x^2y^2/4]}{6\pi^2 x(1-y^2)} \times$$

$$\left(2 + \frac{N_\nu(g_V^2+g_A^2) + 2(g_V+g_A)[1-s(1-x)/M_Z^2]}{[1-s(1-x)/M_Z^2]^2 + \Gamma_Z^2/M_Z^2}\right) \quad (4)$$

neglecting radiative corrections (discussed below).

In (4), G_F is the Fermi coupling constant, α is the fine structure constant, s is the square of the centre-of-mass energy, x is the photon energy in units of the incident beam energy, $y = \cos\vartheta_\gamma$ is the cosine of the polar angle of the photon with respect to the incident beam direction, N_ν is the number of low-mass neutrino generations, and M_Z and Γ_Z are the mass and the total width of the Z^0. For M_Z and Γ_Z, the averages of measurements by the four LEP experiments, as quoted in reference [15], are used, i.e., $M_Z = 91.1888 \pm 0.0044$ GeV and $\Gamma_Z = 2.4974 \pm 0.0038$ GeV. In the Standard Model [16], $g_V = -\frac{1}{2} + 2\sin^2\vartheta_W$ and $g_A = -\frac{1}{2}$, where ϑ_W is the weak mixing angle. The "2" term in (4) is from the square of the t-channel W-exchange amplitude, the $N_\nu(g_V^2+g_A^2)$ term is the dominant one and

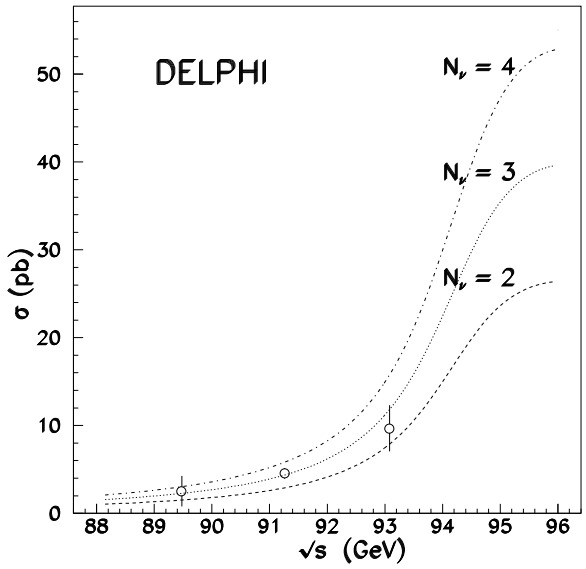

Fig. 4. Measured cross-sections for the reaction $e^+e^- \to \nu\bar{\nu}\gamma$ with $E_\gamma >$ 3 GeV and $|\cos\vartheta_\gamma| < 0.7$, including all corrections and background subtractions. The *dashed*, *dotted*, and *dot-dashed curves* show the expectations for two, three and four generations respectively

is from the square of the s-channel Z^0 amplitude, and the $2(g_V + g_A)[...]$ term is from WZ^0 interference.

Thus the cross-section for $e^+e^- \to \nu\bar{\nu}\gamma$ may be calculated if the analytic formula is integrated over the appropriate kinematic region. The integration may be performed either numerically or by generating $\nu\bar{\nu}\gamma$ events by Monte Carlo techniques and recording the fraction that survives the kinematic cuts. Here, numerical integration over the allowed fiducial region is used to calculate the cross-sections, and the generation of events by Monte Carlo techniques is used to determine the efficiencies. Radiative corrections must also be included. They modify (4) both in line shape and in cross-section [17]. But since in the reaction $e^+e^- \to \nu\bar{\nu}\gamma$ there is no final state radiation, and therefore no interference between initial and final state radiation, the uncertainties are small.

The results of the calculations of $e^+e^- \to \nu\bar{\nu}\gamma$ [17] and $e^+e^- \to e^+e^-\gamma$ [13], and the calculation of the cross-section for $e^+e^- \to \nu\bar{\nu}\gamma$ based on the number of observed events, are shown in Table 3. Note that the calculated radiative Bhabha background is not proportional to the integrated luminosity at each centre-of-mass energy. This is because, for the 1994 data sample, the replacement of the SAT luminosity monitor with the STIC luminosity monitor closed the gap between the luminosity monitor and the FEMC calorimeter, as discussed in Sect. 2. Consequently the peak between 6 and 9 GeV in the radiative Bhabha background (see Fig. 3) comes only from the 1993 data.

Figure 4 shows the measured values of the cross-section for $e^+e^- \to \nu\bar{\nu}\gamma$ in the accepted region, i.e. $E_\gamma > 3$ GeV and $|\cos\vartheta_\gamma| < 0.7$, at the three centre-of-mass energies. The curves show the integral of the theoretical calculations [17] over the region of the cuts. A fit to the three data points with N_ν left as a free parameter yielded

$$N_\nu = 2.89 \pm 0.32(stat) \pm 0.19(syst)$$

as the number of light neutrino generations. The χ^2 was 0.7 for two degrees of freedom. Systematic uncertainties common to the three data points were removed before the fit, and then included in the total systematic error. Contributions to the quoted systematic uncertainty are ± 0.07 background subtractions, ± 0.14 trigger efficiency, ± 0.08 reconstruction efficiency, ± 0.08 visual scan: all other contributions are negligible in comparison. This result is consistent with that found by other methods, and also by this method by the other LEP collaborations [18].

6 Searches for new physics

Events featuring a single highly energetic photon can provide evidence for the presence of new physics. In the selected sample, presented in Sect. 3, a total of 11 single photon events have $E_\gamma > 10$ GeV, while 4 have $E_\gamma > 15$ GeV. A total of 8.2 such events is expected with $E_\gamma > 10$ GeV, and 2.9 events with $E_\gamma > 15$ GeV, from the neutrino counting reaction $e^+e^- \to \nu\bar{\nu}\gamma$ [17] assuming 3 light neutrino generations. All other backgrounds are negligible above 10 GeV. No event is observed with $E_\gamma > 22$ GeV. Thus these data show no evidence for any anomalous source of high energy single photons.

This result is consistent with the results of the other LEP collaborations [19]. In the following, limits on possible sources of new physics will be determined on the basis of these observations, taking into account the rates expected from the known sources, $e^+e^- \to \nu\bar{\nu}\gamma$ with $N_\nu = 3$ and $e^+e^- \to e^+e^-\gamma$.

6.1 Limit on excited neutrinos

Excited neutrinos can be produced at LEP either in pairs through the reaction $e^+e^- \to \nu^*\bar{\nu}^*$, or singly through the reaction $e^+e^- \to \nu^*\bar{\nu}$ [9].

The cross-section for pair production is independent of the compositeness scale Λ, and present LEP limits already exclude this channel for excited neutrino masses M_{ν^*} below $\sqrt{s}/2$ [20].

The single production of excited neutrinos, which depends on the $Z\nu^*\bar{\nu}$ couplings, allows the lower limit on the branching fraction of the Z^0 into $\nu^*\bar{\nu}$ to be extended to values of M_{ν^*} up to M_Z. With the assumption of a pure left-handed or right-handed ν^*, the cross-section for $Z^0 \to \nu^*\bar{\nu}$ is just the $Z^0 \to \nu\bar{\nu}$ cross-section [21], apart from kinematical factors,

$$\frac{\sigma_{\nu^*\bar{\nu}}}{\sigma_{\nu\bar{\nu}}} = \frac{s}{\Lambda^2}\left(1 - \frac{M^2_{\nu^*}}{s}\right)^2\left(1 + 2\frac{M^2_{\nu^*}}{s}\right) \qquad (5)$$

Events with single ν^* production were generated for a number of M_{ν^*} values. The branching fraction of ν^* into $\nu\gamma$ was assumed to equal unity, and a $(1 + \cos\alpha)$ angular distribution was assumed for the radiative decay of the ν^*, where α is the polar angle of the neutrino in the ν^* rest frame, defined with respect to the ν^* momentum direction in the centre-of-mass frame. Using the efficiencies thus calculated, the observation of no events with $E_\gamma > 22$ GeV yields the

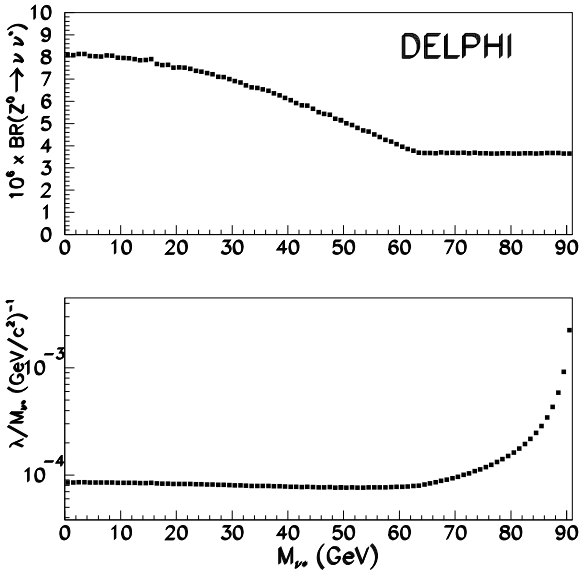

Fig. 5. Upper limits at 95% confidence level on BR($Z^0 \rightarrow \nu^*\bar{\nu}$) and λ/M_{ν^*} as functions of M_{ν^*}

upper limit at 95% confidence level for the branching ratio BR($Z^0 \rightarrow \nu^*\bar{\nu}$) as a function of M_{ν^*} shown in Fig. 5 (upper plot). The limit is approximately constant for high M_{ν^*} values, where all photons from ν^* decay exceed 22 GeV. The corresponding upper limit on the effective coupling constant λ/M_{ν^*}, defined as [22]

$$\frac{\lambda}{M_{\nu^*}} = \frac{1}{\sqrt{2}\Lambda} \tag{6}$$

is given in Fig. 5 (lower plot).

6.2 Limit on the tau neutrino magnetic moment

The magnetic moment coupling of the tau neutrino gives a contribution to the differential cross-section for the process $e^+e^- \rightarrow \nu\bar{\nu}\gamma$ of the form [10]

$$\frac{d\sigma}{dxdxdy} = \frac{\alpha^2\kappa^2}{96\pi}\mu_B^2 C[\chi_W]F[s,x,y] \tag{7}$$

where x is the photon energy in units of the incident beam energy, y is the cosine of the photon polar angle with respect to the beam axis, and κ is the anomalous magnetic moment of the tau neutrino in units of the Bohr magneton, μ_B. The kinematics are contained in the function

$$F[s,x,y] \equiv (\frac{s^2}{4}) \cdot \frac{1 - x + x^2(1-y^2)/8}{(s - M_Z^2)^2 + M_Z^2\Gamma_Z^2} \tag{8}$$

and the coefficient $C[\chi_W]$ is given by

$$C[\chi_W] \equiv \frac{8\chi_W^2 - 4\chi_W + 1}{\chi_W^2(1-\chi_W)^2} \tag{9}$$

with $\chi_W \equiv \sin^2\vartheta_W$ and using the Standard Model Ze^+e^- and $Z\nu\bar{\nu}$ couplings. Initial state radiation is neglected in the above formulation. Photon and W exchange graphs contribute about 1% in the kinematic region of interest, and have also been neglected.

If the tau neutrino magnetic moment were $\mu_\nu = 5 \times 10^{-6}\mu_B$, then 90% of the increase over the Standard Model prediction would be in the energy region above 22 GeV.

After integrating equation (7) over the kinematically allowed region, with $E_\gamma > 22$ GeV and $|\cos\vartheta_\gamma| < 0.7$, the estimated cross-section expected due to a neutrino magnetic moment at $\sqrt{s} = M_Z$ is

$$\sigma = 6.6 \text{ mb} \times \kappa^2 \tag{10}$$

Taking into account the other two centre-of-mass energy points and correcting for initial state radiation, the observation of no events with $E_\gamma > 22$ GeV yields a limit on an anomalous magnetic moment for ν_τ of

$$\kappa < 5.1 \times 10^{-6} \tag{11}$$

at the 95% confidence level. A similar measurement has been reported by the L3 collaboration [23], and a comparable result has been obtained by combining data from several lower energy e^+e^- experiments [24]. A more stringent limit ($\kappa < 5.4 \times 10^{-7}$) has been obtained by a different technique using the BEBC bubble chamber [25]. It is worth noting that, since the photons considered are real, all these limits apply at $Q^2 = 0$. Existing limits on electron and muon neutrino magnetic moments are already sufficiently stringent to totally preclude any observable effect in this data sample.

6.3 Search for γ'X' production

A new particle 'X' may be produced in association with a photon in the reaction $e^+e^- \rightarrow \gamma$'X'. If 'X' is invisible, or can decay invisibly, it could be seen in the single photon topology. Figure 6a shows the distribution in recoil mass against the photon for the 106 single photon events. The distribution is consistent with that expected from known sources.

Figure 6b shows the resulting upper limit at 95% confidence level on the cross-section for $e^+e^- \rightarrow \gamma$'X' as a function of the mass of the 'X' particle. The limit was calculated using a Poisson distribution taking into account both the expected background and the experimental resolution σ (the points in Fig. 6b are at the centres of bins of width $\pm 1\sigma$). The natural width of the 'X' was assumed to be small compared with the resolution and its production angular distribution was assumed to be isotropic. The limit shown for masses between 40 and 55 GeV is equally valid for masses below 40 GeV. As it is based on a slightly higher integrated luminosity (67.6 pb^{-1} instead of 40.5 pb^{-1}), the limit obtained is slightly more restrictive than that found by OPAL [26].

7 Conclusions

Data are presented on the reaction $e^+e^- \rightarrow \gamma$ + no other detected particle at centre-of-mass energies of 89.48, 91.26, and 93.08 GeV. The measured cross-section for this reaction is used to determine the number of light neutrino generations

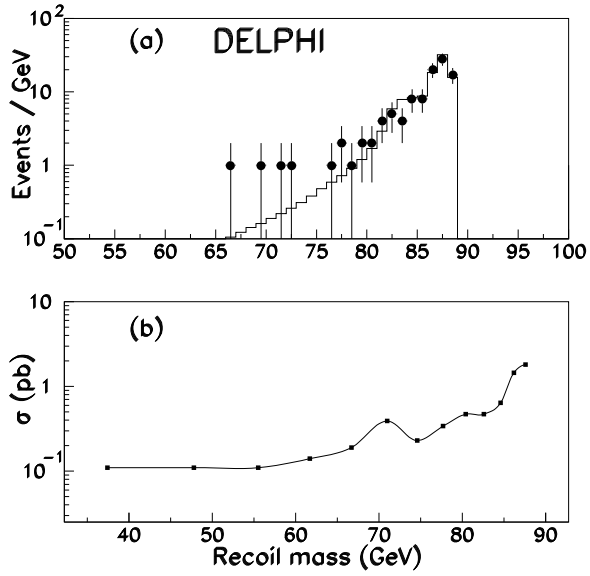

Fig. 6. a Recoil mass distribution for the 106 single photon events with photon energy above 3 GeV (*points*) compared with the expectation for $\nu\bar{\nu}\gamma$ with N_ν = 3 plus the known background processes (*histogram*). **b** Upper limit at the 95% confidence level for the production cross-section of γ'X'

which couple to the Z^0 boson. The result is $N_\nu = 2.89 \pm 0.32(stat) \pm 0.19(syst) = 2.89 \pm 0.38$. No evidence is found for sources of highly energetic single photons other than the known Standard Model processes; upper limits at the 95% confidence level are consequently set on the production of excited neutrinos (see Fig. 5), on the production of an invisible particle 'X' via the reaction $e^+e^- \rightarrow \gamma$'X' (see Fig. 6b), and on a possible tau neutrino magnetic moment ($\kappa < 5.1 \times 10^{-6}$ at the 95% confidence level).

Acknowledgements. We are greatly indebted to our technical collaborators and funding agencies for their support in building and operating the DELPHI detector, and to the members of the CERN-SL Division for the excellent performance of the LEP collider.

References

1. P. Aarnio, et. al., DELPHI Coll., Nucl. Instr. and Meth. **A303** (1991) 233
2. P. Abreu, et al., DELPHI Coll., Nucl. Instr. and Meth. **A378** (1996) 57
3. E. Ma and J. Okada, Phys. Rev. Lett. **41** (1978) 287
4. K. J. F. Gaemers, R. Gastmans, and F. M. Renard, Phys. Rev. **D19** (1979) 1605
5. G. Barbiellini, B. Richter, and J. L. Siegrist, Phys. Lett. **106B** (1981) 414
6. J. Bartels, A. Fridman, A. Schwarz, and Tai Tsun Wu, Z. Phys. **C23** (1984) 295
7. M. Caffo, R. Gatto, and E. Remiddi, Phys. Lett. **B173** (1986) 91
8. Elmar Lieb, "Radiative Neutrinozählung mit dem DELPHI-Detektor auf der Z^0-Resonanz", Diplomarbeit, Bergische Universität - Gesamthochschule Wuppertal, WU D 88 - 30 (1988)
9. F. Boudjema and Djouadi, Phys. Lett. **B240** (1990) 485
10. Thomas M. Gould and I. Z. Rothstein, Phys. Lett. **B333** (1994) 545
11. H. G. Fischer, Nucl. Instr. and Meth., **A265** (1988) 218; F. L. Navarria, et al., Nucl. Instr. and Meth., **A257** (1987) 499; A. Cattai, et al., Nucl. Instr. and Meth., **A235** (1985) 310; E. I. Rosenberg, "The DELPHI High Density Projection Chamber", in Proceedings of the Gas Sampling Calorimetry Workshop II, Fermilab, Batavia, Il. (1985) 450; H. G. Fischer and O. Ullaland, IEEE Trans. Nucl. Sci., **NS-27** (1980) 38
12. D. Gillespie and T. Malmgren, "The First and Second Level HPC Trigger Simulation", DELPHI 94-46 CAL 155, 2 May 1994
13. For the generator of the process $e^+e^- \rightarrow \nu\bar{\nu}\gamma$, see F. A. Berends, et al., Nucl. Phys. **B301** (1988) 583, and R. Miquel, C. Mana and M. Martinez, Z. Phys. **C48** (1990) 309. For radiative corrections, see C. Mana and M. Martinez, Nucl. Phys. **B287** (1987) 601, and F. A. Berends et al., Nucl. Phys. **B301** (1988) 583. For radiative corrections to the background processes $e^+e^- \rightarrow e^+e^-\gamma$, $\gamma\gamma$, or $\gamma\gamma\gamma$, see F. A. Berends, K. J. F. Gaemers and R. Gastmans, Nucl. Phys. **B57** (1973) 381, **B63** (1973) 381, and **B68** (1979) 541; F. A. Berends and R. Kleiss, Nucl. Phys. **B177** (1981) 237 and **B186** (1981) 22; and Dean Karlen, Nucl. Phys. **B289** (1987) 23. For the KORALZ generator, see S. Jadach, B. F. L. Ward and Z. Was, Comp. Phys. Comm. **66** (1991) 276
14. For $e^+e^- \rightarrow \mu^+\mu^-\gamma$, see J. Bartels, et al., Z. Phys. **C23** (1984) 295. The contribution to the background from $e^+e^- \rightarrow \tau^+\tau^+\gamma$ with the photon within the cuts and none of the charged particles from the tau decays vetoing the event is even smaller than that from $e^+e^- \rightarrow \mu^+\mu^-\gamma$. For $e^+e^- \rightarrow \gamma\pi^0$, $\gamma n\bar{n}$, and $\gamma\pi^0\pi^0$, see E. Ma and J. Okada, Phys. Rev. Lett. **41** (1978) 287
15. D. Schaile, in "Proceedings of the XXVII International Conference on High Energy Physics", 20-27 July 1994, Glasgow, Scotland, UK, page 27
16. S. L. Glashow, Nucl. Phys. **B22** (1961) 579; S. Weinberg, Phys. Rev. Lett. **19** (1967) 1264; A. Salam, Proceedings of the 8th Nobel Symposium, p. 367, May 1968, Ed. N. Svartholm, New York, Wiley 1968
17. O. Nicrosini and L. Trentadue, Phys. Lett. **B196** (1987) 551; O. Nicrosini and L. Trentadue, Nucl. Phys. **B318** (1989) 1
18. D. Buskulic, et al. ALEPH Coll., Phys. Lett. **B313** (1993) 520; B. Adeva, et al. L3 Coll., Phys. Lett. **B275** (1992) 209; O. Adriani, et al. L3 Coll., Phys. Lett. **B292** (1992) 463; M. Z. Akrawy, et al., OPAL Coll., Z. Phys. **C50** (1991) 373; R. Akers, et al., OPAL Coll., Z. Phys. **C65** (1995) 47
19. O. Adriani, et al., L3 Coll., Phys. Lett. **B297** (1993) 469; R. Akers, et al., op. cit., see previous reference
20. D. Decamp, et al., ALEPH Coll., Phys. Lett. **B250** (1990) 172; P. Abreu, et al., DELPHI Coll., Phys. Lett. **B274** (1992) 230; D. Bertrand, et al., DELPHI Coll., "Search for an Excited Neutrino Using the DELPHI Detector", DELPHI 92-111 Dallas PHYS 217; B. Adeva, et a., L3 Coll., Phys. Lett. **B252** (1990) 525
21. K. Hagiwara, S. Komamiya and Z. Zeppenfeld, Z. Phys. **C29** (1985) 115
22. P. Abreu, et al., DELPHI Coll., Z. Phys. **C53** (1992) 41
23. M. Acciarri, et al., L3 Coll., Phys. Lett. **B346** (1995) 190. For a direct comparison with this L3 result, the DELPHI limit corresponds to $\kappa < 4.4 \times 10^{-6}$ at the 90% confidence level
24. H. Grotch and R. W. Robinett, Z. Phys. **C39** (1988) 553
25. A. M. Cooper-Sarkar, et al., Phys. Lett. **B280** (1992) 153
26. R. Akers, et al., op. cit., see reference [18]